Tertiary and Quaternary Structural Changes in $G_{i\alpha 1}$ Induced by GTP Hydrolysis

Mark B. Mixon, Ethan Lee, David E. Coleman, Albert M. Berghuis,* Alfred G. Gilman, Stephen R. Sprang†

Crystallographic analysis of 2.2 angstrom resolution shows that guanosine triphosphate (GTP) hydrolysis triggers conformational changes in the heterotrimeric G-protein α subunit, $G_{i\alpha 1}$. The switch II and switch III segments become disordered, and linker II connecting the Ras and α helical domains moves, thus altering the structures of potential effector and βγ binding regions. Contacts between the α-helical and Ras domains are weakened, possibly facilitating the release of guanosine diphosphate (GDP). The amino and carboxyl termini, which contain receptor and βγ binding determinants, are disordered in the complex with GTP, but are organized into a compact microdomain on GDP hydrolysis. The amino terminus also forms extensive quaternary contacts with neighboring α subunits in the lattice, suggesting that multimers of α subunits or heterotrimers may play a role in signal transduction.

Two recognized checkpoints in the G protein signal transduction cycle correspond to reciprocal conformational transformations in the G_α subunit. First, the GDP-bound G protein must interact with a ligand-activated receptor molecule before G_α can exchange GDP product for GTP substrate. GTP destabilizes the ground state of the subunit and promotes dissociation of activated G_α from the receptor and $G_{\beta\gamma}$. The metastable, activated GTP-bound α subunit then modulates the activities of downstream effectors such as adenylyl cyclase or phospholipase Cβ (*1–3*). Second, the lifetime of the active G_α·GTP signaling species is limited by its intrinsic, or in some cases effector stimulated (*4*), rate of GTP hydrolysis. Catalysis is hindered by the exquisite complementarity of the enzyme to its substrate and product, requiring conformational changes en route to the transition state (*5*, *6*) and possibly, release of phosphate from the GDP·Mg^{2+}·Pi product complex as well (*7*). After hydrolysis, inactive, GDP-bound G_α associates with heterodimers of β and γ subunits ($G_{\beta\gamma}$) and is subsequently unable to interact with effectors. $G_{\beta\gamma}$ complexes either act with G_α as coregulators of effectors (*8*, *9*) or function independently as signaling molecules in other pathways (*10*, *11*).

M. B. Mixon, D. E. Coleman, and S. R. Sprang are in the Department of Biochemistry and E. Lee and A. G. Gilman are in the Department of Pharmacology, University of Texas Southwestern Medical Center, 5323 Harry Hines Boulevard, Dallas, TX 75235–9050, USA. A. M. Berghuis and S. R. Sprang are also with the Howard Hughes Medical Institute at the University of Texas Southwestern Medical Center, 5323 Harry Hines Boulevard, Dallas, TX 75235–9050, USA.

*Present address: Department of Biochemistry, McMaster University, 1200 Main Street West, Hamilton, Ontario, Canada L8N 3Z5

†To whom correspondence should be addressed.

Crystallographic analysis of transducin α ($G_{t\alpha}$) truncated at the amino terminus and bound to magnesium–guanosine 5′-O-3-thiotriphosphate (GTPγS·Mg^{2+}) (*12*) and of the complex with GDP·Mg^{2+} (*13*) demonstrates that GTP hydrolysis leads to extensive conformational changes in residues that surround the catalytic site. These are propagated along elements of secondary structure and alter potential effector binding surfaces (*14*). After hydrolysis, the ground state of the system is restored by reassociation of the α subunit with βγ subunits. The NH_2-terminus of the α subunit is required for $G_{\beta\gamma}$ binding, whereas the COOH-terminus forms part of the receptor recognition site (*15*). The recently determined structure of the intact $G_{i\alpha 1}$·GTPγS·Mg^{2+} complex indicates that both termini are completely disordered in the activated state (*5*).

Although it is normally assumed that G_α·GDP associates with $G_{\beta\gamma}$ to form monomeric $G_{\alpha\beta\gamma}$ heterotrimers, results indicate that both G_α and $G_{\alpha\beta\gamma}$ might form multimeric complexes. Rodbell and his colleagues have detected large polydisperse arrays of G_i, G_o, and G_s in detergent extracts of plasma membranes. These complexes apparently contained GDP-bound α subunits and do not form in the membrane preparations exposed simultaneously to activated receptor ligands and GTPγS (*16–19*). Likewise, multimers of G_t heterotrimers can be crosslinked to cyclic guanosine monophosphate (GMP) phosphodiesterase in the presence of GDP, but not after activation with stable GTP analogs (*20*). Photoactivation-crosslinking of $G_{t\alpha}$ results in the formation of α subunit dimers and trimers (*21*).

We now describe the three-dimensional structure of the intact α subunit of $G_{i\alpha 1}$ (40.5 kD) bound to GDP. The protein was crystallized in the absence of magnesium, which binds to $G_{i\alpha 1}$ only weakly in the presence of GDP (*22*). Coupled to α_2 adrenergic, M_2 muscarinic cholinergic, and other receptors, G_i inhibits adenylate cyclase (*2*). The structural data presented below show that GTP hydrolysis is accompanied by conformational changes in effector binding surfaces and the transition of the amino and carboxyl termini to an ordered state. The ordered terminal residues participate in an unexpected quaternary interaction between α subunits that could provide a structural basis for the possible formation of higher order G protein complexes.

Structure determination. In the early stages of the structural analysis, the model of the GDP bound form of $G_{i\alpha 1}$ was derived from analysis of crystals of the $Gly^{203} \rightarrow$ Ala mutant (G203A $G_{i\alpha 1}$), because these crystals diffracted to higher resolution than did crystals of the wild-type protein. The G203A $G_{i\alpha 1}$ mutant, which corresponds to $Gly^{226} \rightarrow$ Ala in $G_{s\alpha}$ (*23*), cannot undergo the conformational rearrangements required to dissociate from $G_{\beta\gamma}$ subsequent to binding GTP and is thus inactive in vivo. The GDP complexes of both the mutant and wild-type proteins were crystallized in the absence of Mg^{2+} (*24*). Crystals of wild-type and G203A $G_{i\alpha 1}$ are isomorphous (*25*), and the structures of the two proteins proved to be virtually identical. Using atomic coordinates of $G_{i\alpha 1}$·GTPγS·Mg^{2+} (*26*) as a search model, we obtained an initial crystallographic model for the G203A $G_{i\alpha 1}$·GDP complex by molecular replacement (*25*). After cycles of model-building and refinement, the structure of the G203A mutant, refined to a resolution of 2.6 Å, was used as starting model to complete and refine the atomic model of $G_{i\alpha 1}$·GDP to 2.2 Å (Table 1).

The model of the $G_{i\alpha 1}$·GDP complex includes residues 9 to the COOH-terminus of the intact 354-residue polypeptide chain, one molecule of GDP bound to the catalytic site, and 70 ordered water molecules. The model also contains one sulfate ion within the NH_2-terminal region. The coordinate set has been refined to a final *R* factor of 0.218 for all data in the resolution range 6.0 to 2.2 Å (R_{free} = 0.291). The overall B factor for backbone atoms in the model is 38.5 $Å^2$, and several regions of the molecule are either completely disordered or correspond to weak or poorly connected electron density. These fully or partially disordered segments are not represented in the final model and include residues 1 to 8, 202 to 217, and 234 to 239. The last two regions correspond, respectively, to most of the α2 helix contained within the switch II region and the switch III loop as described in $G_{t\alpha}$ (*12*). PROCHECK analysis (*27*) demon-

strates that no residues occupy disallowed main chain conformations; more than 92 percent of the nonglycine residues fall within the most favored regions of the Ramachandran plot (*28*).

Nucleotide binding and conformational changes in the switch regions. The overall fold of $G_{i\alpha1}$·GDP is nearly identical to that of $G_{i\alpha1}$·GTPγS·Mg^{2+} (*5*), $G_{t\alpha}$·GTPγS·Mg^{2+} (*12*), and $G_{t\alpha}$·GDP·Mg^{2+} (*13*). The molecule is divided into two domains: a GTP-binding module (9 to 56 and 188 to 354) that is similar to the canonical Ras-like α-β structure found in many GTP binding proteins, and a large α-helical domain (63 to 176) that is inserted into the Ras domain and is present only in heterotrimeric G proteins (Fig. 1). Although the overall fold of the molecule is preserved, the structure of $G_{i\alpha1}$ in the inactive, GDP-bound state differs in several respects from that of the active GTPγS·Mg^{2+} complex. In particular, the 25 residues extending from Asp^{9} to Glu^{33} together with the 11 COOH-terminal residues fold into a compact microdomain at the NH_2-terminal edge of the Ras domain β sheet.

Several segments of the polypeptide chain surrounding the catalytic site assume different conformations after GTP hydrolysis. To describe these changes, we follow the switch I–switch III nomenclature first used in reference to $p21^{ras}$ (*29*) and $G_{t\alpha}$ (*13*) (Fig. 1). Switch I corresponds to residues 177 to 187, the second polypeptide segment that connects the Ras and helical domains (also called linker 2). Switch II is the α2 helix and preceding loop (residues 199 to 219), and switch III is an extended turn between β4 and α3 (residues 231 and 242) that forms some of the contacts between the Ras and helical domains. $G_{t\alpha}$ (*13*) also exhibits conformational changes in corresponding regions, but they differ qualitatively from those observed in $G_{i\alpha1}$. We define a new segment, switch IV, encompassing residues 111 to 119 that connect αB and αC in the helical domain, and which also undergoes structural rearrangements. All of the nucleotide-dependent structural changes, both tertiary and quaternary, appear to be conformationally coupled.

When individual segments that undergo major rearrangements (9 to 33, 111 to 119, 179 to 184, 201 to 219, 231 to 241, and 344 to 354 are excluded), superposition of the static secondary structural elements in the $G_{i\alpha1}$·GDP and $G_{i\alpha1}$·GTPγS·Mg^{2+} complexes reveals a root-mean-square (rms) deviation of only 1.11 Å between corresponding Cα atoms. However, superimposed independently, the cores of the α-helical (63 to 111 and 119 to 176) and Ras (34 to 52, 187 to 197, 220 to 229, and 242 to 343) domains show even smaller deviations of 0.63 and 0.51 Å, respectively (Fig. 2). Relative to $G_{i\alpha1}$·GTPγS·Mg^{2+}, the α-helical domain is rotated by 4.2° with respect to the Ras domain (Fig. 2). The interdomain rotation may be a consequence of both the extensive packing interactions formed between molecules in the lattice and the loss of interdomain contacts, as described below.

Interactions between the protein and the nucleoside moiety are nearly identical in the GDP and GTPγS·Mg^{2+} complexes (Fig. 3). Similarly, the nucleotide-binding segments in the active site remain essentially the same, with the exception of linker 2–switch I and the α2–switch II helix. As noted in the structures of Ras (*29*) and G_t (*13*), the con-

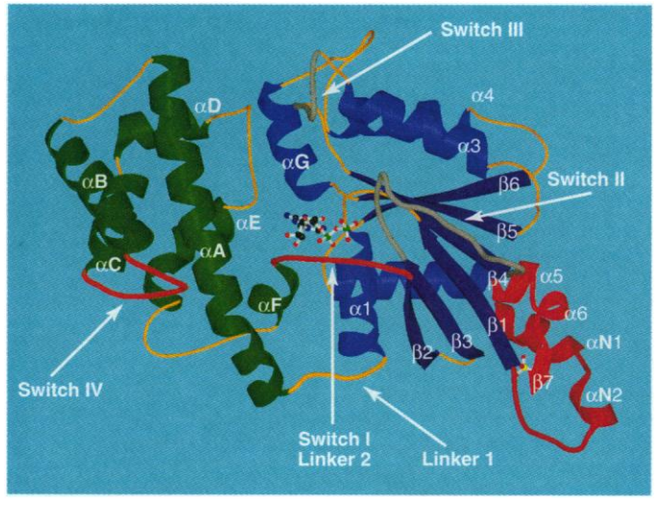

Fig. 1. Overall structure of $G_{i\alpha1}$·GDP. The α-helical domain and Ras-like domain are colored green and blue, respectively. Secondary structural elements that have undergone conformational changes from the active (GTPγS) to the inactive (GDP) state are represented in red; those that become disordered are colored in gray. The nucleotide is positioned between the two domains and is drawn as a ball-and-stick model. The ribbon diagram of $G_{i\alpha1}$·GDP was generated with Molscript (*49*) and rendered with Raster3D (*50*).

Table 1. Data reduction and refinement statistics for wild type and G203A $G_{i\alpha1}$. Crystals of $G_{i\alpha1}$·GDP and G203A $G_{i\alpha1}$·GDP were transferred into stabilizing solution and equilibrated in cryosolvent (*25*) before the data were collected. Both crystals belong to space group *I*4; $G_{i\alpha1}$ cell constants, $a = b = 121.8$ Å, $c = 68.4$ Å; G203A $G_{i\alpha1}$, $a = b = 121.7$ Å, $c = 68.4$ Å. A cooling system (Molecular Structure Corporation) maintained the crystals at 110 K throughout data collection. Native data sets were measured with a RAXIS-IIC detector with CuKα x-rays generated by a Rigaku RU300 rotating anode source and focused with a mirror system (Molecular Structure Corporation) in combination with a 0.0008-inch nickel filter. The raw data were integrated and scaled by means of DENZO and SCALEPACK (*55*). Molecular replacement calculations were performed in X-PLOR v3.1 (*52*) with G203A $G_{i\alpha1}$ data to 4.0 Å resolution and the coordinates of $G_{i\alpha1}$·GTPγS·Mg^{2+} (ordered solvent molecules and GTPγS·Mg^{2+} were omitted) as the search model (*5, 26*). After cycles of rigid-body refinement (*26*) with data in the resolution range 10 Å to 3.2 Å, conformational shifts in switch IV (residues 111 to 119) and the ordered NH_2- and COOH-termini could be identified in sigma-A–weighted (*56*) maps. Changes were made to the model by means of the electron density and modeling program O (*57*), and the process of refinement continued with iterative cycles of Powell minimization and grouped *B*-factor refinement, incorporating the data to 2.6 Å resolution (*52*). SigmaA weighted, simulated annealing "OMIT" maps were used to refit extensive sections of the model. The model-building and refinement process was guided throughout by monitoring the free *R* factor. The refined model of G203A $G_{i\alpha1}$·GDP was used as a starting point for the structure solution and refinement of the wild-type $G_{i\alpha1}$·GDP complex. Cycles of manual refitting, simulated annealing (*58*), and Powell minimization with the data set extending from 6.0 Å and 2.2 Å were undertaken to remove any residual model bias carried over from the G203A $G_{i\alpha1}$ model. Although the data in the highest resolution shell, given in parentheses, are weak, they contributed marginally to the quality of the final electron density map. Seventy water molecules were identified in difference and $(2F_{obs} - F_c)$ Fourier maps by peak intensity, stereochemical, and hydrogen bonding criteria, and their positions and thermal parameters were refined.

Measurement	Protein	
	Wild type	G203A
Resolution Å	6.0–2.2 (2.3–2.2)	8.0–2.6 (2.7–2.6)
$I_o/\sigma I_o$	12.0 (2.4)	21.9 (3.5)
Completeness (%)	95.0 (70.6)	99.2 (95.2)
R_m*	0.052 (0.412)	0.053 (0.352)
R_{free}	0.291 (0.356)	0.280 (0.395)
R factor	0.218 (0.352)	0.217 (0.341)
Reflections (*N*)	22840 (1977)	13409 (1347)
Observations (*N*)	81724	39340
rms bond angle (°)‡	1.804	1.826
rms bond distance (Å)‡	0.018	0.013

*$R_m = \Sigma|I - \langle I\rangle|/\Sigma\langle I\rangle$; *R* factor $= \Sigma|F_o - F_c|/\Sigma F_c$; R_{free} corresponds to the *R* factor for 10 percent of the reflections in the data set excluded from refinement (*54*). Only data greater than 2.0 $F/\sigma(F)$ are included in the *R*-factor statistics. ‡Root-mean-square deviation of bond angle or bond length from ideality (*28*).

formational changes in these two regions result directly from the loss of the γ phosphate and the magnesium ion. In the active structure, Thr^{181} in switch I coordinates the essential Mg^{2+} ion, which in turn is partially responsible for binding and stabilizing the γ phosphate. As in $G_{t\alpha}$·GDP, the backbone of the switch I region drops away from the nucleotide. The conformational change in this segment is centered on the Cα of Lys^{180}, which pulls away by more than 2 Å from its position at the active site of the GTPγS·Mg^{2+} complex. The adjacent residue, Thr^{181}, also swings out and thereby disrupts part of the ligand sphere that tightly coordinates the magnesium ion. A direct contact between the side chain of Asn^{76} in the α-helical domain and the backbone of switch I is also weakened in the inactive structure. However, the conformational change in switch I cannot be attributed to the absence of Mg^{2+} in these crystals because, in the presence of 5 mM Mg^{2+}, a $G_{i\alpha1}$·GDP·Mg^{2+} complex is formed but the position of switch I is unaltered (*30*). In part, as described below, the shift in switch I may be correlated with the formation of quaternary interactions between $G_{i\alpha1}$ subunits.

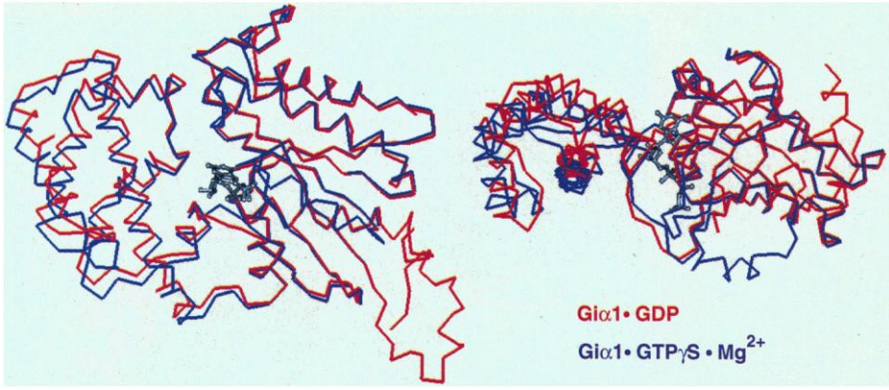

Fig. 2. Superposition of the active $G_{i\alpha1}$·GTPγS·Mg^{2+} and inactive $G_{i\alpha1}$·GDP structures. Two orthogonal views of superimposed α subunits, $G_{i\alpha1}$·GTPγS·Mg^{2+} (blue) and inactive $G_{i\alpha1}$·GDP (red), related by a 90-degree rotation about the horizontal axis. Superposition of the two Ras-like domains yield an rms deviation of 1.11 Å.

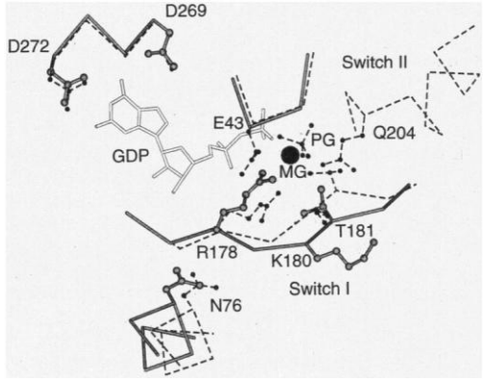

Fig. 3. Changes in and around the active site following hydrolysis. The magnesium (MG) ligation sphere in the active structure (dashed) is disrupted by the absence of the nucleotide γ phosphate (PG) and rearrangements in switch I. The loss of stabilizing contacts with PG also results in a completely disordered switch II in the (solid) inactive structure. This diagram (also Figs. 4, 5a, and 7) was generated by means of Setor and plotted in Setorplot (*51*).

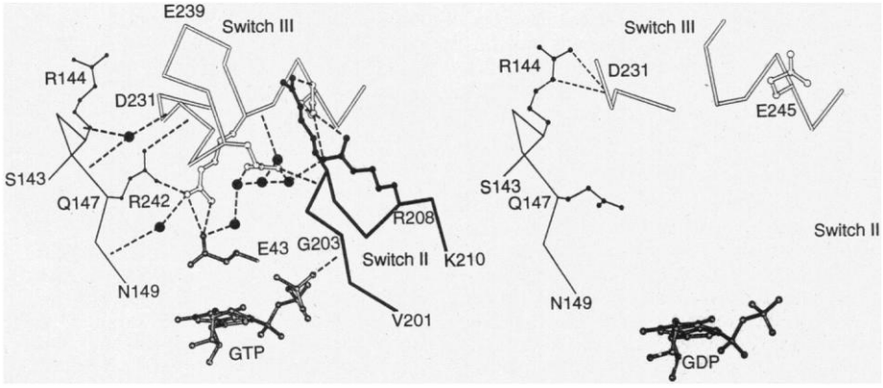

Fig. 4. Disruption of interdomain contacts triggered by the loss of γ phosphate. Two highly conserved arginines (205 and 208) in the active GTPγS·Mg^{2+} structure (**left**) form important electrostatic interactions between switch II and switch III. The switch III loop (Val^{233} to Arg^{242}) in turn makes contacts with the α-helical domain via a water-mediated hydrogen bonding network and through interactions between Arg^{144} and Asp^{231}. With the exception of the later contact, all hydrogen bonds between switch III and the α-helical domain are lost in the GDP complex (**right**).

With GDP in the active site, a dianionic phosphate group occupies the position taken by the monoionic β phosphate in the $G_{i\alpha1}$·GTPγS·Mg^{2+} complex. As partial compensation, Arg^{178} drops into a position that parallels the α and β nucleotide phosphates, thereby stabilizing the product complex (Fig. 3). In this configuration, the arginine guanidinium group forms hydrogen bonds with an oxygen from each phosphate group. However, as in the GTPγS·Mg^{2+} complex, the Arg^{178} side chain in the GDP-bound structure is characterized by high thermal parameters. The flexibility of Arg^{178} in the latter two structures is in marked contrast with its behavior in the transition-state analog complex ($G_{i\alpha1}$·GDP·AlF_4^-) (*5*) in which it adopts a well-ordered conformation. Arg^{178} appears to exert its primary effect on catalysis during the formation of the transition state. Glu^{43}, which pairs with Arg^{178} in $G_{i\alpha1}$·GTPγS·Mg^{2+} is disordered in the GDP complex. Concomitant with the loss of the hydrogen bond between the amide of Gly^{203} in switch II and the γ phosphate of GTP, the α2 helix (residues 201 to 218), which contains the critical catalytic residue Gln^{204}, is completely disordered (Fig. 3). There is no evidence of any ordered structures between residues 201 and 218 in $G_{i\alpha1}$·GDP.

The collapse of the α2 helix destabilizes other regions of the structure. In the GTPγS·Mg^{2+} conformation, two arginines (Arg^{205} and Arg^{208}) in α2 provide important stabilizing contacts to switch III (Glu^{236} and Glu^{245}) via a conserved network of ionic interactions (*12*) (Fig. 4). Other residues in the switch III loop (Asp^{231}, Val^{233}, and Arg^{242}) contribute to the stable active conformation of the loop through interactions with the α-helical domain (Arg^{144} and Gln^{147}), either directly or through two ordered waters (OH_2 405 and OH_2 453) positioned between the two domains. Unsupported by stabilizing contacts with switch II, the switch III loop assumes a highly mobile conformation, and the residues between Val^{233} and Met^{240} are disordered in the GDP bound protein (Fig. 4). With the rearrangement of switch III, the three stable polar interdomain contacts made in that region in the active structure are reduced to contacts between a single

residue pair ($Arg^{144} \rightarrow Asp^{231}$ backbone) in the inactive, GDP-bound state. The remaining residues participating in interdomain hydrogen bonds also show an increase in thermal disorder. Linker 1 and linker 2 (switch I), the two peptide segments that join the Ras and α-helical domains, have temperature factors that are well above the mean for the structure. The loss of discrete interdomain contacts and the increase in the thermal parameters of interfacial residues are consistent with the rapid dissociation of GDP from $G_{i\alpha1}$ relative to GTPγS. The importance of even a single interdomain contact in maintaining the integrity of the active site in $G_{s\alpha}$ was illustrated by disruption of a salt bridge formed by Lys^{278} and Asp^{158} (equivalent to Lys^{270} to Asp^{150} in $G_{i\alpha1}$). Mutating one of the residues was sufficient to block the ability of AlF_4^-, but not GTPγS, to effect a conformational change in the α subunit necessary for stimulation of adenylyl activity cyclase activity (*31*). The transition from order to disorder appear to be structurally concerted, and they are confined to residues on the one face of the G_α subunit that is implicated in effector binding (*14*).

A terminal microdomain and the formation of $G_{i\alpha1}$ oligomers. In contrast to the switch II region implicated in effector binding, the NH_2- and COOH-terminal residues involved in receptor and $G_{\beta\gamma}$ binding are well ordered in the GDP-bound state. Disordered in $G_{i\alpha1}$·GTPγS·Mg^{2+}, these residues fold into a compact microdomain in $G_{i\alpha1}$·GDP (Fig. 1). Although residues 1 to 8 remain disordered, the eight that follow fold into a three-turn α helix (αN1, residues Asp^9 to Asp^{16}) which is interrupted by a 90° bend before terminating with a single, four-residue 3_{10} helix (αN2, residues 20 to 23). The following seven residues form a loop that is connected directly to the β1 strand, extending it by three residues. At the COOH-terminus, α5, which is disordered after residue 343 in the GTPγS·Mg^{2+} complex, is extended by three residues and continues for another eight residues to form a structure that is cradled between the NH_2-terminus and the body of the Ras domain. It is supported by van der Waals interactions and hydrogen bonds with β1 on one side and αN1 on the other. The α5 helix is interrupted by a 90° kink at residue Gln^{347} and continues for a single turn of 3_{10} helix (Leu^{348} to Asp^{350}). The polypeptide chain is terminated by a one-residue β extension at Leu^{353} that pairs with the NH_2-terminus of β1 (Arg^{32}) to form a short antiparallel ribbon. In this context, the ADP-ribosylation factor 1·GDP (ARF) complex appears to have a similar helical conformation of NH_2-terminal residues (*32*).

The NH_2-terminal segment of the microdomain is stabilized, and possibly nucleated, by a network of interactions between a cluster of basic residues and a tightly bound sulfate ion (Fig. 5). Arginines 15 and 21, which are conserved in the G_i, G_o, and G_t subfamily, are oriented to form a typical binding pocket (*33*, *34*) for the sulfate ion (derived from the crystallization solution). Each of the interactions between arginine and SO_4^{-2} interactions appear to stabilize the two helices αN1 and αN2, that form in the GDP-bound subunit. The sulfate ion also anchors a third conserved Arg^{32}. In addition to contacting the sulfate ion, Arg^{32} bridges the NH_2-terminus and the COOH-terminus by contributing to a hydrogen bond network that indirectly links Asp^{20} to the backbone of Cys^{351}. Since sulfate ions are capable of binding at phosphate ion binding sites (*35*), it is possible that inorganic phosphate is bound to the microdomain under physiological conditions.

An intriguing interaction occurs between the NH_2-terminal (αN1 and αN2) helices of one $G_{i\alpha1}$ subunit and the α-helical domain of a neighboring molecule related by a twofold screw axis (Fig. 6 and Table

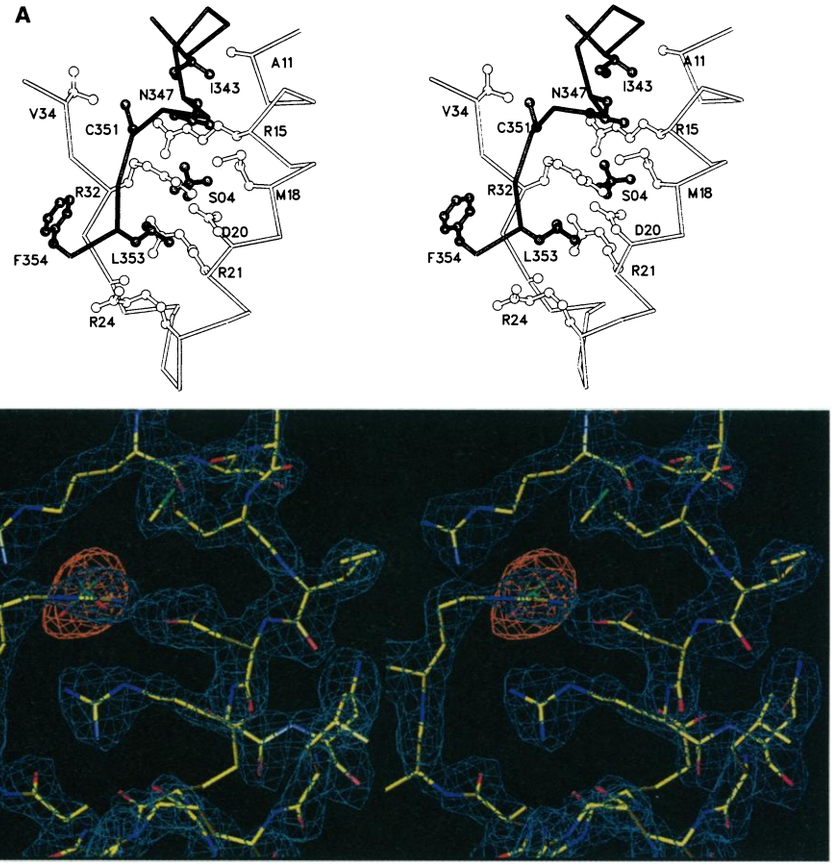

Fig. 5. NH_2-terminal and COOH-terminal microdomain. (**A**) Portions of the NH_2- (light) and COOH- (dark) terminal peptides form a microdomain in the GDP complex. The configuration is stabilized through complementary polar and nonpolar interactions. (**B**) A stereo diagram of $2F_o - F_c$ electron density map contoured at 1.5 σ around the NH_2- and COOH-termini (blue) and the sulfate ion (orange).

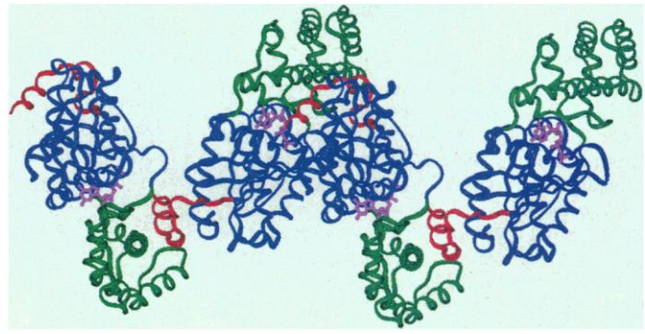

Fig. 6. Lattice interaction. The α subunits are organized in a "head-to-tail" oligomer in the crystal lattice. Each subunit is related to the next by a twofold screw rotation that positions the NH_2-terminus (red) from the Ras-like domain (blue) of one subunit into the α-helical domain (green) of the adjacent subunit. The position of the nucleotide (magenta) is also shown.

2). When viewed parallel to the long axis of αA, the helical domain resembles a C clamp (Fig. 2). A head-to-tail dimer of $G_{i\alpha 1}$ subunits is formed when the arms of the C clamp of one subunit embrace the NH_2-terminus of the adjacent subunit. The pattern of association is repeated by lattice symmetry, to generate a helical array of α subunits in the crystal (Fig. 6).

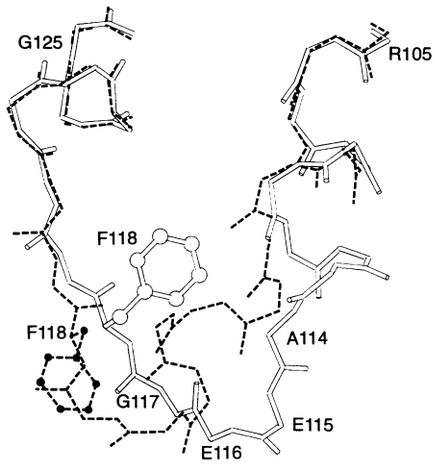

Fig. 7. Switch IV conformational change. The formation of α-subunit oligomers is accompanied by a conformational change in switch IV. In the conformation of the GDP complex (solid), the loop connecting αB and αC is extended, allowing residues at the apex of the loop to form contacts with the NH_2-terminus of an adjacent subunit. Phe^{118} pivots from an exposed position in the GTPγS·Mg^{2+} conformation (dashed) to the interior of the loop to form part of the structural core of the contact.

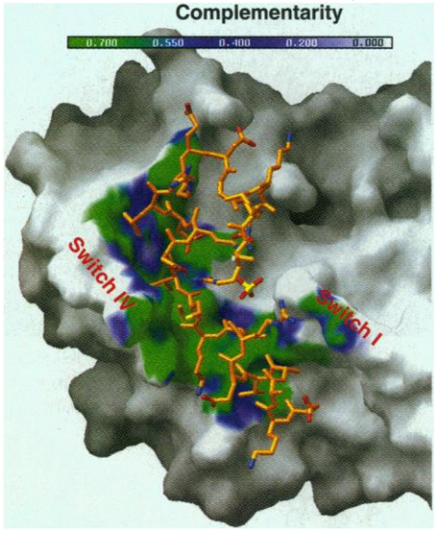

Fig. 8. The α-helical domain and the NH_2-COOH–terminal microdomain form an extensive interface. The molecular surface [generated with the program GRASP (*60*)] of the α-helical domain is colored according to the complementarity index, Sc, computed with software as described by Lawrence *et al.* (*38*). Regions of high complementarity (green = >0.7) comprise the inner surface of the contact region and are surrounded by areas of moderate complementarity (blue = 0.7–0.4). The total solvent-accessible surface area occluded from solvent contact upon formation of the interface is 1617 Å.

The conformational change in the switch IV peptide (Figs. 2 and 7) facilitates the quaternary interaction. The αB helix of the α-helical domain unwinds by approximately one turn, extending the αB-αC loop toward the αN1 binding surface, and creates one of the two arms of the α-domain "C clamp". Unwinding of the αB helix causes Phe^{118} to flip into the αB-αC turn, forming a hydrophobic core for the expanded loop (Fig. 7). In this configuration, residues Phe^{108}, Ala^{111}, Gly^{112}, A^{114}, Glu^{115}, Glu^{116}, and Gly^{117} of switch IV make several contacts with the microdomain of the adjacent molecule (Table 2). The conformation of the αB-αC corner in $G_{i\alpha 1}$·GDP is similar to that in $G_{t\alpha}$ in both the GDP·Mg^{2+} and GTPγS·Mg^{2+} bound states (*12*, *13*). The rearrangement of switch I also contributes to the formation of the G_α-G_α interface by forming the second arm of the C clamp (Fig. 2).

The contact between G_α subunits has a number of properties suggesting that it is not an artifact of the crystallization conditions. First, the total solvent-accessible surface area (*36*) occluded by formation of the $G_{i\alpha 1}$ dimer (1617 $Å^2$) is comparable to that buried by complexes between monoclonal antibodies and their protein antigens and between specific protein-protein recognition sites (*37*). Second, the complementarity of the interacting surfaces, as assessed by the numerical index of Colman *et al.* (*38*), is comparable to that computed for physiologically relevant protein complexes (Fig. 8). The interface is held together by a mixture of polar and nonpolar residues (Table 2). Two hydrophobic residues in the interface that are notably conserved in the G_α family (Ile^{19} and Leu^{23}) form contacts with switch IV, one of two elements in the interface that undergoes a conformational change. Third, several of the conformational changes attributed to GTP hydrolysis, notably, the creation of the terminal microdomain and rearrangements in switch I, appear to be directly coupled with G_α oligomerization in the crystals. Fourth, neither the conformational differences nor the quaternary interactions that distinguish the $G_{i\alpha 1}$·GDP crystals from those of the $G_{i\alpha 1}$·GDPγS·Mg^{2+} complex can be attributed to differences in crystallization conditions. Crystals of both types can be grown and stabilized under similar conditions. We infer that the structural differences between the GDP and GTPγS·Mg^{2+} complexes are a direct consequence of the nucleotide species bound to the active site.

Reciprocal, GDP-GTP–dependent order-disorder transitions in βγ and effector binding surfaces. Hydrolysis of GTP to

Table 2. Contacts between α subunits involve the αA helix, switch I and switch IV peptides of one molecule ("origin subunit", left column), with residues of a second, 2_1-related "contacting" subunit molecule in the crystal lattice (second column). Residue names are given in the standard one-letter code for amino acids. The numbers in parentheses separated by a slash "/" associated with each residue in the right-hand column ("contacting subunit") indicate the number of polar and van der Waals contacts, repectively, that it forms with the residue of the origin subunit listed in the same row, left column. Polar contacts include hydrogen bonds and ion pairs. Hydrogen bonds are defined as potential donor-acceptor distances less than 3.5 Å with appropriate stereochemistry (*59*). Ion pairs have contact distances between charged atoms in acidic and basic side chains less than 3.5 Å. The van der Waals nonpolar interactions include all other nonbonded contacts less than 4.0 Å. The interface comprises 54 nonpolar and 8 polar interactions. Abbreviations for the amino acid residues are: A, Ala; C, Cys; D, Asp; E, Glu; F, Phe; G, Gly; H, His; I, Ile; K, Lys; L, Leu; M, Met; N, Asn; P, Pro; Q, Gln; R, Arg; S, Ser; T, Thr; V, Val; W, Trp; and Y, Tyr.

Origin subunit	Contacting subunit
αA	
Y69	V13 (0/2)
S75	S16 (1/1), K17 (0/1), M18 (1/0), I19 (0/1)
Q79	N22 (0/7)
I82	N22 (0/2)
R86	N22 (2/1), L23 (0/1), R24 (0/1), E25 (0/2)
Switch IV	
F108	L23 (0/2)
A111	I19 (0/1), L23 (0/1)
G112	L23 (0/2)
A114	I19 (0/3)
E115	M18 (0/2), I19 (1/1), K349 (0/3)
E116	K17 (0/4), K349 (1/4)
G117	K17 (1/1)
Switch I	
V179	A12(0/3), S16(0/5)
K180	A12(0/2), S16(1/0)
T182	K192(0/3)

GDP triggers structural changes in $G_{i\alpha1}$ that are manifested functionally by a loss of affinity for effectors and an increased affinity for βγ (although it is not yet clear whether hydrolysis itself or release of Pi is the critical event). The interaction between the γ phosphate of the nucleotide and the amide nitrogen of Gly^{203} in the α2 helix may be regarded as the structural linchpin that stabilizes the active (GTP-bound) conformation (*29*). Dissolution of this key interaction as a result of the hydrolytic activity of the enzyme leads to reciprocal changes in the affinity of G_α for effectors and βγ. The structure of $G_{i\alpha1}$·GDP described here demonstrates that destabilization of switch II after P_i release is accompanied by conformational changes in the switch I and switch III regions that are in direct or GTP-mediated contact with switch II. These structural changes may contribute to the loss of effector binding activity. Whereas the NH_2-terminus is disordered in crystals of $G_{i\alpha1}$·GTPγS·Mg^{2+}, it is possible that this segment assumes an ordered conformation when myristoylated and palmitoylated in vivo and, as evidence suggests (*39*, *40*), may be involved in effector activation in the GTP bound state of $G_{i\alpha1}$.

The terminal microdomain that is partly assembled in the GDP state is proposed to contain the $G_{\beta\gamma}$ binding surface. Deletion of the ~2 kD of NH_2-terminal fragment from $G_{s\alpha}$ (*41*), $G_{t\alpha}$ (*42*), and $G_{o\alpha}$ and $G_{i\alpha}$ (*43*, *44*) results in the loss of affinity for $G_{\beta\gamma}$. Further, deletion of residues 7 to 10 drastically impairs the ability of $G_{o\alpha}$ to bind $G_{\beta\gamma}$. In the $G_{i\alpha1}$·GDP structure, residues 1 to 8 are disordered. If the αN1 helix were to be extended from residue 9 toward the NH_2-terminus, it would pack against the COOH-terminal α5 helix, which has been implicated in receptor interactions (*3*). In $G_{o\alpha}$, Cys^{215} can be cross-linked to $G_{\beta\gamma}$, suggesting that the α2 helix (switch II) might also form part of, or lie in close proximity to, the $G_{\beta\gamma}$ binding site. Not only does this region overlap partially with a putative effector binding domain, it is also located on the opposite side of the subunit from the NH_2-terminus. Hence, $G_{\beta\gamma}$ may wrap around the α subunit. It is also possible that the NH_2-terminus adopts a different conformation in the heterotrimer, as suggested by the apparent inaccessibility of the site of pertussis toxin–mediated ADP ribosylation (Cys^{351}) in the free $G_{i\alpha1}$·GDP structure shown (Fig. 5B).

A role for G_α oligomerization in vivo. Interactions between α subunits could generate G protein heterotrimeric clusters or α subunit clusters around receptor molecules (*45*). In a membrane environment where the concentration of macromolecules is high, the kinetics of interactions between receptor and G protein is likely to be diffusion-limited. Formation of multimeric complexes of G protein would overcome the limitation by allowing a single receptor to interact with a locally concentrated pool of α subunits and, in this way, attain rapid signal amplification. Studies of interactions between rhodopsin and G_t have shown that receptor-catalyzed nucleotide exchange is cooperative with respect to the concentration of $G_{t\alpha}$ (*46*), with an apparent Hill constant of 2, suggesting that two or more $G_{t\alpha}$ subunits could interact with receptor. The addition of βγ magnified the sigmoidal response.

The observation that a dimer of α subunits responds to receptor suggests that G_α-G_α interactions could promote GDP-GTP exchange through a cycle that bypasses the normal requirement for βγ. The formation of the NH_2- and COOH-terminal microdomain involved in polymer formation may also contribute to the loss of interactions between the Ras and α-helical domains observed here, thereby facilitating the release of GDP. Similarly, excision of the α-helical domain in $G_{s\alpha}$ accelerates the dissociation rate of guanine nucleotide (*47*). The two major contributors to the dimer contact, the NH_2-terminus and the α-helical domain, are both remote from the active site and yet both have been identified as important modulators of the rate of GDP dissociation in $G_{i\alpha2}$ (*48*).

A nucleotide exchange mechanism that is independent of βγ could amplify hormonal signals in a pathway that is ancillary to the normal G protein cycle. However, the structural data do not exclude the possibility that the terminal microdomain could mediate GDP-dependent oligomerization among G protein heterotrimers, as suggested by Rodbell (*19*). At this point, however, the prospect of G_α or $G_{\alpha\beta\gamma}$ oligomerization is an intriguing possibility that remains to be confirmed by rigorous evidence obtained in vivo.

REFERENCES AND NOTES

1. A. G. Gilman, *Annu. Rev. Biochem.* **56**, 615 (1987).
2. J. R. Hepler and A. G. Gilman, *Trends Biochem. Sci.* **17**, 383 (1992).
3. E. J. Neer, *Cell* **80**, 249 (1995).
4. G. Berstein *et al.*, *ibid.* **70**, 411 (1992).
5. D. E. Coleman *et al.*, *Science* **265**, 1405 (1994).
6. J. Sondek, D. G. Lambright, J. P. Noel, H. E. Hamm, P. B. Sigler, *Nature* **372**, 276 (1994).
7. A. Berghuis, E. Lee, D. E. Coleman, A. G. Gilman, S. R. Sprang, in preparation.
8. W.-J. Tang and A. G. Gilman, *Science* **254**, 1500 (1991).
9. A. V. Smrcka and P. C. Sternweis, *J. Biol. Chem.* **268**, 9667 (1993).
10. D. E. Clapham and E. J. Neer, *Nature* **365**, 403 (1993).
11. K. D. Wickman *et al.*, *ibid.* **368**, 255 (1994).
12. J. P. Noel, H. E. Hamm, P. B. Sigler, *ibid.* **366**, 654 (1993).
13. D. G. Lambright, J. P. Noel, H. E. Hamm, P. B. Sigler, *ibid.* **369**, 621 (1994).
14. B. R. Conklin and H. R. Bourne, *Cell* **73**, 631 (1993).
15. B. R. Conklin, O. Chabre, Y. H. Wong, A. D. Federman, H. R. Bourne, *J. Biol. Chem.* **267**, 31 (1992).
16. S.-I. Nakamura and M. Rodbell, *Proc. Natl. Acad. Sci. U.S.A.* **87**, 6413 (1990).
17. ———, *ibid.* **88**, 7150 (1991).
18. S. Coulter and M. Rodbell, *ibid.* **89**, 5842 (1992).
19. S. Jahangeer and M. Rodbell, *ibid.* **90**, 8782 (1993).
20. V. N. Hingorani, D. T. Tobias, J. T. Henderson, Y.-K. Ho, *J. Biol. Chem.* **263**, 6916 (1988).
21. R. R. Vaillancourt, N. Dhanasekaran, G. L. Johnson, A. E. Ruoho, *Proc. Natl. Acad. Sci. U.S.A.* **87**, 3645 (1990).
22. T. Higashijima, K. M. Ferguson, P. C. Sternweis, M. D. Smigel, A. G. Gilman, *J. Biol. Chem.* **262**, 762 (1987).
23. E. Lee, R. Taussig, A. G. Gilman, *ibid.* **267**, 1212 (1992).
24. D. E. Coleman *et al.*, *J. Mol. Biol.* **238**, 630 (1994).
25. Crystals of $G_{i\alpha1}$·GDP and G203A $G_{i\alpha1}$·GDP grown in the absence of Mg^{2+} (*24*) were transferred into a stabilization solution consisting of 70 percent saturated $LiSO_4$, 100 mM *N*,*N*-bis-[2-hydroxyethyl]-2-aminoethanesulfonic acid (BES), pH 7.0, 5 mM dithiothreitol, and 5 mM EDTA (buffer A). Before the data were collected, crystals of suitable dimensions (usually 500 to 600 μm by 100 μm) were transferred at 30-minute intervals through a series of drops that consisted of the stabilization solutions supplemented with increasing amounts (Δ5 percent) of glycerol. After the final infiltration with 20 percent glycerol in buffer A, the crystals were mounted in a rayon loop and frozen in liquid nitrogen for data collection.
26. Molecular replacement calculations were performed in X-PLOR v3.1 (*52*) using G203A $G_{i\alpha1}$ data to 4.0 Å resolution and the coordinates of $G_{i\alpha1}$·GTPγS·Mg^{2+} (ordered solvent molecules and GTPγS·Mg^{2+} were omitted) as the search model (*5*). The correct solution produced by Patterson correlation (PC) refinement (*53*) corresponding to an 8.8-σ peak in the rotation function (the highest false peak was 3.5 σ). An *R*-factor translation search based on the rotation solution yielded a 16.9-σ peak with the highest false peak appearing at 3 σ above the mean. These gave crystallographic *R* factors of R_{free} = 46.7 and R_{work} = 44.2, where R_{free} is calculated on the basis of 10 percent of the data removed from the refinement calculations (*54*) and R_{work} is computed with the remaining reflections of the "working set". The molecular replacement model was subjected to rigid-body least-squares refinement with data in the resolution range 10 Å to 3.2 Å initially with the use of the entire molecule as a single rigid unit. In subsequent cycles, the Ras domain (residues 33 to 54 and 183 to 343) and the α-helical domain (residues 55 to 182) were treated as rigid bodies. In the last cycles, individual α-helical and β-strand secondary structural elements were treated as separate rigid-body units.
27. R. A. Laskowski, M. W. MacArthur, D. S. Moss, J. M. Thornton, *J. Appl. Cryst.* **26**, 283 (1993).
28. R. A. Engh and R. Huber, *Acta Cryst.* **A47**, 392 (1991).
29. M. V. Milburn *et al.*, *Science* **247**, 939 (1990).
30. D. E. Coleman and S. R. Sprang, unpublished data.
31. J. Codina and L. Birnbaumer, *J. Biol. Chem.* **269**, 29339 (1994).
32. J. C. Amor, D. H. Harrison, R. A. Kahn, D. Ringe, *Nature* **372**, 704 (1994).
33. P. Chakrabarti, *J. Mol. Biol.* **234**, 463 (1993).
34. R. R. Copley and G. J. Barton, *ibid.* **242**, 321 (1994).
35. D. Barford and L. N. Johnson, *Nature* **340**, 609 (1971).
36. B. Lee and F. M. Richards, *J. Mol. Biol.* **55**, 379 (1971).
37. J. Janin and C. Chothia, *J. Biol. Chem.* **265**, 16027 (1990).
38. M. C. Lawrence and P. M. Colman, *J. Mol. Biol.* **234**, 946 (1993).
39. R. Taussig, J. A. Iñiguez-Lluhi, A. G. Gilman, *Science* **261**, 218 (1993).
40. C. Kleuss and A. G. Gilman, unpublished data.
41. R. Taussig, W.-J. Tang, J. R. Helper, A. G. Gilman, *J. Biol. Chem.* **269**, 6093 (1994).
42. S. E. Navon and B. K.-K. Fung, *ibid.* **262**, 15746 (1987).
43. R. Graf, R. Mattera, J. Codina, M. Estes, L. Birnbaumer, *ibid.* **267**, 24307 (1992).

44. E. J. Néer, L. Pulsifer, L. G. Wolf, *ibid.* **263**, 8896 (1988).
45. M. Rodbell, *Curr. Topics Cell. Reg.* **32**, 1 (1992).
46. M. Wessling-Resnick and G. L. Johnson, *J. Biol. Chem.* **262**, 3697 (1987).
47. D. W. Markby, R. Onrust, H. R. Bourne, *Science* **262**, 1895 (1993).
48. S. Osawa, N. Dhanasekaran, C. W. Woon, G. L. Johnson, *Cell* **63**, 697 (1990).
49. P. J. Kraulis, *J. Appl. Cryst.* **24**, 946 (1991).
50. D. Bacon and W. F. Anderson, *J. Mol. Graphics* **6**, 219 (1988).
51. S. V. Evans, *ibid.* **11**, 134 (1993).
52. A. T. Brünger, *X-PLOR Version 3.1. A System for X-ray Crystallography and NMR* (Yale Univ. Press, New Haven, CT, 1992).
53. ———, *Acta Crystallogr.* **A46**, 46 (1990).
54. ———, *Nature* **355**, 472 (1992).
55. Z. Otwinowski, in *Data Collection and Processing*, L. Sawyer, N. Isaacs, S. W. Bailey, Eds. (Science and Engineering Council, UK, 1993), p. 56.
56. R. J. Read, *Acta Crystallogr.* **A42**, 140 (1986).
57. T. A. Jones and M. Kjeldgaard, *O Version 5.6* (Department of Molecular Biology, Uppsala University, Uppsala, Sweden, 1990); unpublished material.
58. A. T. Brünger, J. Kuriyan, M. Karplus, *Science* **235**, 458 (1987).
59. E. N. Baker and R. E. Hubbard, *Prog. Biophys. Mol. Biol.* **44**, 97 (1984).
60. A. Nicholls, GRASP: Graphical Representation and Analysis of Surface Properties (Columbia University, New York, 1992).
61. Supported by NIH grant DK 46371, Welch Foundation grant I-1229 (S.R.S.), NIH grant GM34497, American Cancer Society grant BE30-O, Welch Foundation grant I-1271, the Lucille P. Markey Charitable Trust, and the Raymond Willie Chair of Molecular Neuropharmacology. Coordinates have been deposited with the Protein Data Bank, accession code number 1GDD.

30 June 1995; accepted 2 October 1995

AAAS–Newcomb Cleveland Prize

To Be Awarded for a Report, Research Article, or an Article Published in *Science*

The AAAS–Newcomb Cleveland Prize is awarded to the author of an outstanding paper published in *Science*. The value of the prize is $5000; the winner also receives a bronze medal. The current competition period began with the 2 June 1995 issue and ends with the issue of 31 May 1996.

Reports, Research Articles, and Articles that include original research data, theories, or syntheses and are fundamental contributions to basic knowledge or technical achievements of far-reaching consequence are eligible for consideration for the prize. The paper must be a first-time publication of the author's own work. Reference to pertinent earlier work by the author may be included to give perspective.

Throughout the competition period, readers are invited to nominate papers appearing in the Reports, Research Articles, or Articles sections. Nominations must be typed, and the following information provided: the title of the paper, issue in which it was published, author's name, and a brief statement of justification for nomination. Nominations should be submitted to the AAAS–Newcomb Cleveland Prize, AAAS, Room 924, 1333 H Street, NW, Washington, DC 20005, and **must be received on or before 30 June 1996**. Final selection will rest with a panel of distinguished scientists appointed by the editor-in-chief of *Science*.

The award will be presented at the 1997 AAAS annual meeting. In cases of multiple authorship, the prize will be divided equally between or among the authors.